面向大尺度战场的信道仿真加速算法

刘 畅 李维实 徐 强* 时成哲 邵士海
(电子科技大学通信抗干扰全国重点实验室 成都 611731)

摘 要：大尺度战场环境中电磁频谱作战装备测试和演训需要依靠大规模数字化电磁环境进行仿真，然而大尺度电磁信道计算复杂度较高，难以提升计算速度。针对这一问题，该文提出一种迭代时域辐射度算法。该算法通过递推方法建模信道，利用空间相干性复用前一时刻的信道数据，并经过修正后用于当前时刻的信道计算。同时，采用面元信道搜索方法对面元中的信道进行低复杂度近似，有效降低了计算复杂度。仿真结果表明，与传统时域辐射度算法相比，所提算法在保证计算精度的基础上计算速度提升了1个数量级。与频域辐射度算法相比，所提算法的时延分辨率更高，更适用于大规模战场环境。

关键词：信道仿真；室外传播；辐射度算法
中图分类号：TN92 **文献标识码**：A **文章编号**：1009-5896(2025)00-0001-08
DOI: 10.11999/JEIT240655

1 引言

在大尺度战场环境下开展电磁频谱作战装备的测试、演训，组织复杂且成本极高[1,2]，因此美国国防部立项研究数字射频战场模拟器系列项目[3]，旨在建立大规模数字化电磁环境，接入电磁频谱作战相关用频装备，进行装备测试、作战任务演训。

从大尺度电磁信道计算建模角度来看，为真实反映战场实际地形对信道的影响，需要计算当前时刻设备所在位置的确定性信道[4,5]。由于大尺度战场环境的复杂性，确定性信道的计算量较大[6]。目前研究者常采用射线追踪等确定性信道算法[7]来进行反射信道计算。由于射线追踪法主要计算信道的镜面反射，为补充场景中不规则和粗糙表面引起的漫反射信道分量，文献[8]引入辐射度算法，并与射线追踪法结合使用进行信道计算。辐射度算法是一种基于能量传播的物理模型，通过将场景中的反射体转换为离散面元，并计算这些面元产生的反射信道。在文献[9,10]中，辐射度算法被用于计算室内外环境下的信道并验证了计算结果的准确性。文献[11]提出了一种计算高次反射信道的时域辐射度算法，并在室外信道计算中得到应用[12]。

但是大尺度战场环境面元数量多，且时域辐射度算法计算复杂度随信道反射次数呈指数增长，其存储空间以及计算时间也显著增加。文献[13]通过简化面元数据结构来加快计算速度，但这种简化方式只适用于特定室内场景，且并没有解决计算复杂度随反射次数增加呈指数增长的问题，加速效果有限。文献[14,15]将辐射度算法从时域转换到频域，提升了计算速度。然而频域辐射度算法时延分辨率受限于快速傅里叶变换(Fast Fourier Transformation, FFT)点数，因此在大尺度战场中该算法的时延分辨率较低。

本文首先对时域辐射度算法中的信道进行递推公式建模，并根据相邻时刻运动设备地理位置变化较小的特性，利用空间相干性复用前一时刻中计算的信道，将其修正后用于当前时刻信道的计算，形成一种面向大尺度战场的迭代时域辐射度算法。仿真测试结果表明：与传统时域辐射度算法相比，所提算法在降低计算复杂度的同时保证了计算精度；相比于频域辐射度算法，所提算法在大尺度战场下能提供更高的时延分辨率。

2 时域辐射度算法的反射信道建模

时域辐射度算法将场景中的反射体转换为离散面元，对其产生的反射信道进行建模，如图1所示。

收发机之间的反射信道$\boldsymbol{H}_{\mathrm{TR}}^{\mathrm{diff}}$可以被视为由场景中各个面元接收到的信道冲激响应，经过反射作用后，最终汇聚于接收机所形成。以面元i为例，其收到来自发射机的直射信道冲激响应以及其他面元反射而来的信道冲激响应，形成的信道总和为$\boldsymbol{H}_i^{\mathrm{diff}}$。面元$i$再将收到的信道冲激响应反射至接收机，形成收发机间的反射信道。该方法定义函数F来表征信道特性[11,14]，一些研究者称其为形状因子。以面元k和面元i之间的形状因子F_{ki}为例，它由衰减分量D_{ki}，时延分量T_{ki}，和可视函数V_{ki}组成

收稿日期：2024-07-26；改回日期：2025-01-22；网络出版：2025-01-25
*通信作者： 徐强 xuqiang06@uestc.edu.cn
基金项目：国家重点研发计划(2023YFF0717700)
Foundation Item: The National Key Research and Development Program of China (2023YFF0717700)

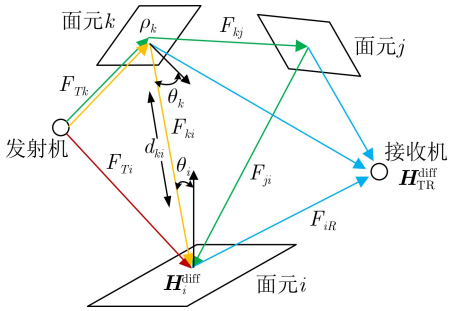

图 1 收发机与场景面元间的反射信道

$$F_{ki}=D_{ki}T_{ki}V_{ki}=\frac{\rho_k\cos\theta_k\cos\theta_i A_i}{\pi d_{ki}^2}\delta(t-\tau_{ki})V_{ki} \quad (1)$$

其中，$\tau_{ki}=\dfrac{d_{ki}}{\mathrm{c}}$ 为传播延时，d_{ki}为面元间的距离，c为光速，ρ_k为反射系数，θ_i和θ_k为面元法向量与两者连线间的夹角，A_i为接收面积，可视函数 $V_{ki}=\begin{cases}0,\text{当面元}k\text{与面元}i\text{之间有阻挡}\\1,\text{当面元}k\text{与面元}i\text{之间没有阻挡}\end{cases}$。发射机与面元$i$的形状因子表示为$F_{\mathrm{T}i}$，面元$i$与接收机的形状因子表示为$F_{i\mathrm{R}}$。

2.1 1次反射信道的建模

以1次反射信道为例，发射机到场景中各面元的直射信道表示为 $\boldsymbol{L}_{\mathrm{T}}=\left[H_{\mathrm{T1}}^{\mathrm{diff0}}\ H_{\mathrm{T2}}^{\mathrm{diff0}}\cdots H_{\mathrm{TN}}^{\mathrm{diff0}}\right]=[F_{\mathrm{T1}}\ F_{\mathrm{T2}}\cdots F_{\mathrm{TN}}]$，而各面元到接收机的直射信道则表示为 $\boldsymbol{L}_{\mathrm{R}}=[F_{1\mathrm{R}}\ F_{2\mathrm{R}}\cdots F_{N\mathrm{R}}]$，其中$N$为面元总数。各面元将来自发射机的直射信道冲激响应向接收机反射，形成收发机间的所有1次反射信道

$$\begin{aligned}\boldsymbol{H}_{\mathrm{TR}}^{\mathrm{diff1}}&=[F_{\mathrm{T1}}*F_{1\mathrm{R}}\ F_{\mathrm{T2}}*F_{2\mathrm{R}}\cdots F_{\mathrm{TN}}*F_{N\mathrm{R}}]\\&=\boldsymbol{L}_{\mathrm{T}}\circledast\mathrm{diag}\left(\boldsymbol{L}_{\mathrm{R}}\right)=\boldsymbol{L}_{\mathrm{T}}\circledast\boldsymbol{L}_{\mathrm{R}}^{\mathrm{diag}}\end{aligned} \quad (2)$$

定义计算对角化函数$\mathrm{diag}\left([c_{1,1}\ c_{1,2}\cdots c_{1,N}]\right)=[c_{1,1}\ c_{1,2}\cdots c_{1,N}]^{\mathrm{diag}}$，其中$c_{1,j}$为分块矩阵中的子矩阵。定义计算$\boldsymbol{C}=\boldsymbol{A}\circledast\boldsymbol{B}$，其中$[\boldsymbol{C}]_{i,j}=\sum_{k=1}^{N}[\boldsymbol{A}]_{i,k}*[\boldsymbol{B}]_{k,j}$。

2.2 多次反射信道的建模

面元k到面元i的1次反射信道为$\boldsymbol{H}_{\mathrm{T}ki}^{\mathrm{diff1}}=F_{\mathrm{T}k}*F_{ki}$，而面元$i$中来自其他面元的1次反射信道可表示为向量$\boldsymbol{H}_{\mathrm{T}i}^{\mathrm{diff1}}=\left[H_{\mathrm{T1}i}^{\mathrm{diff1}}H_{\mathrm{T2}i}^{\mathrm{diff1}}\cdots H_{\mathrm{TN}i}^{\mathrm{diff1}}\right]^{\mathrm{T}}$，因此各面元中的1次反射信道构成一个$N\times N$的矩阵

$$\begin{aligned}\left[\boldsymbol{H}_{\mathrm{T1}}^{\mathrm{diff1}}\cdots\boldsymbol{H}_{\mathrm{TN}}^{\mathrm{diff1}}\right]&=\begin{bmatrix}F_{\mathrm{T1}}\cdots 0\\ \vdots\ \ddots\ \vdots\\ 0\cdots F_{\mathrm{TN}}\end{bmatrix}\circledast\begin{bmatrix}F_{11}\cdots F_{1N}\\ \vdots\ \ddots\ \vdots\\ F_{N1}\cdots F_{NN}\end{bmatrix}\\&=\mathrm{diag}\left(\boldsymbol{L}_{\mathrm{T}}\right)\circledast\boldsymbol{L}_{\mathrm{H}}=\mathcal{F}^{(1)}\left(\boldsymbol{L}_{\mathrm{T}}\right)\end{aligned} \quad (3)$$

定义转移矩阵$\boldsymbol{L}_{\mathrm{H}}$，其元素为面元间形状因子。定义函数$\mathcal{F}(\boldsymbol{A})=\mathrm{diag}\left(\boldsymbol{A}\right)\circledast\boldsymbol{L}_{\mathrm{H}}$，且$\mathcal{F}\left(\begin{bmatrix}\boldsymbol{A}\\ \boldsymbol{B}\end{bmatrix}\right)=\begin{bmatrix}\mathrm{diag}\left(\boldsymbol{A}\right)\circledast\boldsymbol{L}_{\mathrm{H}}\\ \mathrm{diag}\left(\boldsymbol{B}\right)\circledast\boldsymbol{L}_{\mathrm{H}}\end{bmatrix}=\begin{bmatrix}\mathcal{F}\left(\boldsymbol{A}\right)\\ \mathcal{F}\left(\boldsymbol{B}\right)\end{bmatrix}$，并将$\mathcal{F}\left(\mathcal{F}\left(\boldsymbol{A}\right)\right)$记为$\mathcal{F}^{(2)}\left(\boldsymbol{A}\right)$。各面元将来自其他面元的1次反射信道冲激响应向接收机反射，形成收发机间的2次反射信道总和$\boldsymbol{H}_{\mathrm{TR}}^{\mathrm{diff2}}=\mathcal{F}^{(1)}\left(\boldsymbol{L}_{\mathrm{T}}\right)\circledast\boldsymbol{L}_{\mathrm{R}}^{\mathrm{diag}}$。

同理，面元j到面元i的2次反射信道为$H_{\mathrm{T}kji}^{\mathrm{diff2}}=F_{\mathrm{T}k}*F_{kj}*F_{ji}$，面元$i$中来自其他面元的2次反射信道表示为向量$\boldsymbol{H}_{\mathrm{T}i}^{\mathrm{diff2}}=\left[H_{\mathrm{T11}i}^{\mathrm{diff2}}\cdots H_{\mathrm{TN1}i}^{\mathrm{diff2}},\cdots,H_{\mathrm{T1}Ni}^{\mathrm{diff2}}\cdots H_{\mathrm{TN}Ni}^{\mathrm{diff2}}\right]^{\mathrm{T}}$，各面元中的2次反射信道构成一个$N^2\times N$的矩阵

$$\begin{aligned}\left[\boldsymbol{H}_{\mathrm{T1}}^{\mathrm{diff2}}\cdots\boldsymbol{H}_{\mathrm{TN}}^{\mathrm{diff2}}\right]&=\begin{bmatrix}\boldsymbol{H}_{\mathrm{T1}}^{\mathrm{diff1}}\cdots 0\\ \vdots\ \ddots\ \vdots\\ 0\cdots\boldsymbol{H}_{\mathrm{TN}}^{\mathrm{diff1}}\end{bmatrix}\circledast\begin{bmatrix}F_{11}\cdots F_{1N}\\ \vdots\ \ddots\ \vdots\\ F_{N1}\cdots F_{NN}\end{bmatrix}\\&=\mathrm{diag}\left(\mathcal{F}^{(1)}\left(\boldsymbol{L}_{\mathrm{T}}\right)\right)\circledast\boldsymbol{L}_{\mathrm{H}}\\&=\mathcal{F}^{(2)}\left(\boldsymbol{L}_{\mathrm{T}}\right)\end{aligned} \quad (4)$$

各面元中的2次反射信道冲激响应向接收机反射，形成收发机间的3次反射信道总和$\boldsymbol{H}_{\mathrm{TR}}^{\mathrm{diff3}}=\mathcal{F}^{(2)}\left(\boldsymbol{L}_{\mathrm{T}}\right)\circledast\boldsymbol{L}_{\mathrm{R}}^{\mathrm{diag}}$。因此$t_i$时刻收发机间的反射信道总和$\boldsymbol{H}_{\mathrm{TR}}^{\mathrm{difft}_i}$可表示为

$$\begin{aligned}\boldsymbol{H}_{\mathrm{TR}}^{\mathrm{diff}\ t_i}&=\boldsymbol{H}_{\mathrm{TR}}^{\mathrm{diff1}t_i}\oplus\boldsymbol{H}_{\mathrm{TR}}^{\mathrm{diff2}t_i}\oplus\cdots\oplus\boldsymbol{H}_{\mathrm{TR}}^{\mathrm{difft}_i m}\\&=\left(\boldsymbol{L}_{\mathrm{T}}^{t_i}\oplus\mathcal{F}^{(1)}\left(\boldsymbol{L}_{\mathrm{T}}\right)\oplus\cdots\oplus\mathcal{F}^{(m-1)}\left(\boldsymbol{L}_{\mathrm{T}}\right)\right)\\&\quad\circledast\boldsymbol{L}_{\mathrm{R}}^{\mathrm{diag}}\\&=\boldsymbol{K}_m^{t_i}\circledast\boldsymbol{L}_{\mathrm{R}}^{\mathrm{diag}}\end{aligned} \quad (5)$$

定义计算$\boldsymbol{A}\oplus\boldsymbol{B}=\begin{bmatrix}\boldsymbol{A}\\ \boldsymbol{B}\end{bmatrix}$，$m$为反射次数上限，$\boldsymbol{K}_m^{t_i}=\begin{bmatrix}\boldsymbol{L}_{\mathrm{T}}^{t_i}\\ \mathcal{F}^{(1)}\left(\boldsymbol{L}_{\mathrm{T}}^{t_i}\right)\\ \vdots\\ \mathcal{F}^{(m-1)}\left(\boldsymbol{L}_{\mathrm{T}}^{t_i}\right)\end{bmatrix}=\begin{bmatrix}H_{\mathrm{T1}}^{\mathrm{diff0}t_i}\cdots H_{\mathrm{TN}}^{\mathrm{diff0}t_i}\\ \boldsymbol{H}_{\mathrm{T1}}^{\mathrm{diff1}t_i}\cdots\boldsymbol{H}_{\mathrm{TN}}^{\mathrm{diff1}t_i}\\ \vdots\\ \boldsymbol{H}_{\mathrm{T1}}^{\mathrm{diff}(m-1)t_i}\cdots\boldsymbol{H}_{\mathrm{TN}}^{\mathrm{diff}(m-1)t_i}\end{bmatrix}$为$t_i$时刻各面元中的直射信道以及反射次数为$m-1$以下的反射信道。

3 迭代时域辐射度算法

式(5)中$\boldsymbol{K}_m^{t_i}$为各面元中的信道，其规模随反射次数呈指数增长，因此时域辐射度算法的复杂度也随反射次数呈指数增长。本文提出一种改进的时域辐射度算法，本算法将$\boldsymbol{K}_m^{t_i}$的计算转换为递推形式，通过复用上一时刻的计算结果进行计算来减少递推次数，同时结合低复杂度近似方法，有效降低了整体计算的复杂性。

3.1 反射信道的迭代模型

传统时域辐射度算法中，在t_i时刻可通过递推公式进行$m-1$次反射计算得到$\boldsymbol{K}_m^{t_i}$：

$$\begin{aligned}\boldsymbol{K}_m^{t_i} &= \boldsymbol{L}_{\mathrm{T}}^{t_i} \oplus \mathcal{F}\left(\boldsymbol{K}_{m-1}^{t_i}\right)\\ &= \boldsymbol{L}_{\mathrm{T}}^{t_i} \oplus \mathcal{F}\left(\begin{bmatrix}\boldsymbol{L}_{\mathrm{T}}^{t_i}\\ \mathcal{F}^{(1)}\left(\boldsymbol{L}_{\mathrm{T}}^{t_i}\right)\\ \vdots\\ \mathcal{F}^{(m-2)}\left(\boldsymbol{L}_{\mathrm{T}}^{t_i}\right)\end{bmatrix}\right)\\ &= \boldsymbol{L}_{\mathrm{T}}^{t_i} \oplus \begin{bmatrix}\mathcal{F}^{(1)}\left(\boldsymbol{L}_{\mathrm{T}}^{t_i}\right)\\ \mathcal{F}^{(2)}\left(\boldsymbol{L}_{\mathrm{T}}^{t_i}\right)\\ \vdots\\ \mathcal{F}^{(m-1)}\left(\boldsymbol{L}_{\mathrm{T}}^{t_i}\right)\end{bmatrix}\end{aligned} \tag{6}$$

其中，$\boldsymbol{K}_{m-1}^{t_i}$为各面元中反射次数上限为$m-2$的所有信道。在$t_{i+1}$时刻同样需要进行多次递推计算得到 $\boldsymbol{K}_m^{t_{i+1}} = \boldsymbol{L}_{\mathrm{T}}^{t_{i+1}} \oplus \mathcal{F}\left(\boldsymbol{K}_{m-1}^{t_{i+1}}\right)$，而将$\boldsymbol{K}_{m-1}^{t_{i+1}}$替换为$t_i$时刻的计算结果$\boldsymbol{K}_{m-1}^{t_i}$，可以减少递推次数提高计算速度。但相邻时刻$\boldsymbol{L}_{\mathrm{T}}^{t_i}$与$\boldsymbol{L}_{\mathrm{T}}^{t_{i+1}}$的偏差会造成反射信道偏差，需要进行信道修正。

如图2所示，以修正面元k接收到的反射信道$H_{\mathrm{T}jk}^{\mathrm{diff1}\ t_i}$为例：在$t_{i+1}$时刻使用$t_i$时刻的计算结果进行反射计算得到信道为$H_{\mathrm{T}jk}^{\mathrm{diff1}\ t_i} = F_{\mathrm{T}j}^{t_i} * F_{jk}$，而$t_{i+1}$时刻接收到的信道应为$H_{\mathrm{T}jk}^{\mathrm{diff1}\ t_{i+1}} = F_{\mathrm{T}j}^{t_{i+1}} * F_{jk}$。场景中面元间的几何关系是静止固定的，面元之间的形状因子不会随时间发生变化，信道变化来源于发射机移动导致发射机与面元之间直射形状因子$F_{\mathrm{T}j}$随时间变化。因此可以通过获取直射形状因子$F_{\mathrm{T}j}$中时延分量$T_{\mathrm{T}j}$和衰减分量$D_{\mathrm{T}j}$在相邻时刻的变化来完成修正。

具体而言，将t_i时刻直射形状因子中时延分量$T_{\mathrm{T}j}^{t_i} = \delta(t-\tau_{\mathrm{T}j}^{t_i})$和$t_{i+1}$时刻对应的时延分量$T_{\mathrm{T}j}^{t_{i+1}} = \delta(t-\tau_{\mathrm{T}j}^{t_{i+1}})$进行时延值作差，得到时延修正值$T_{\mathrm{mod}} = \delta\left(t-\left(\tau_{\mathrm{T}j}^{t_{i+1}}-\tau_{\mathrm{T}j}^{t_i}\right)\right)$；将$t_i$时刻直射形状因子中衰减分量$D_{\mathrm{T}j}^{t_i}$和$t_{i+1}$时刻对应的衰减分量$D_{\mathrm{T}j}^{t_{i+1}}$作商得到衰减修正值$D_{\mathrm{mod}} = D_{\mathrm{T}j}^{t_{i+1}} \Big/ D_{\mathrm{T}j}^{t_i}$。最后将$D_{\mathrm{mod}}\,T_{\mathrm{mod}}$与$t_i$时刻的信道进行卷积，完成信道的修正，将修正过程定义为modify

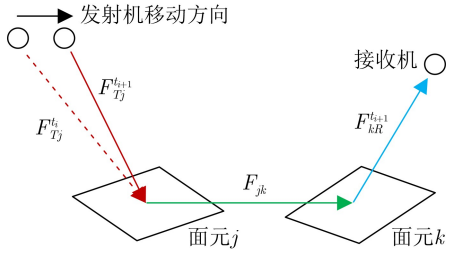

图 2 信道修正示意图

$$H_{\mathrm{T}jk}^{\mathrm{diff1}\ t_{i+1}} = \mathrm{modify}\left(H_{\mathrm{T}jk}^{\mathrm{diff1}\ t_i}\right) = D_{\mathrm{mod}}\,T_{\mathrm{mod}} * H_{\mathrm{T}jk}^{\mathrm{diff1}\ t_i} \tag{7}$$

对$\boldsymbol{L}_{\mathrm{T}}^{t_{i+1}} \oplus \mathcal{F}\left(\boldsymbol{K}_{m-1}^{t_i}\right)$中的$\mathcal{F}\left(\boldsymbol{K}_{m-1}^{t_i}\right)$进行modify修正处理，便可消除信道偏差得到$\boldsymbol{K}_m^{t_{i+1}}$：

$$\begin{aligned}\boldsymbol{K}_m^{t_{i+1}} &= \boldsymbol{L}_{\mathrm{T}}^{t_{i+1}} \oplus \mathrm{modify}\left(\mathcal{F}\left(\boldsymbol{K}_{m-1}^{t_i}\right)\right)\\ &= \boldsymbol{L}_{\mathrm{T}}^{t_{i+1}} \oplus \mathrm{modify}\left(\begin{bmatrix}\mathcal{F}^{(1)}\left(\boldsymbol{L}_{\mathrm{T}}^{t_i}\right)\\ \mathcal{F}^{(2)}\left(\boldsymbol{L}_{\mathrm{T}}^{t_i}\right)\\ \vdots\\ \mathcal{F}^{(m-1)}\left(\boldsymbol{L}_{\mathrm{T}}^{t_i}\right)\end{bmatrix}\right)\\ &= \boldsymbol{L}_{\mathrm{T}}^{t_{i+1}} \oplus \mathrm{modify}\\ &\quad \cdot\left(\begin{bmatrix}\boldsymbol{H}_{\mathrm{T1}}^{\mathrm{diff1}t_i} & \cdots & \boldsymbol{H}_{\mathrm{T2}}^{\mathrm{diff1}t_i}\\ \boldsymbol{H}_{\mathrm{T1}}^{\mathrm{diff2}t_i} & \cdots & \boldsymbol{H}_{\mathrm{T}N}^{\mathrm{diff2}t_i}\\ \vdots & \vdots & \\ \boldsymbol{H}_{\mathrm{T1}}^{\mathrm{diff}(m-1)t_i} & \cdots & \boldsymbol{H}_{\mathrm{T}N}^{\mathrm{diff}(m-1)t_i}\end{bmatrix}\right)\\ &= \boldsymbol{L}_{\mathrm{T}}^{t_{i+1}} \oplus \begin{bmatrix}\boldsymbol{H}_{\mathrm{T1}}^{\mathrm{diff1}t_{i+1}} & \cdots & \boldsymbol{H}_{\mathrm{T2}}^{\mathrm{diff1}t_{i+1}}\\ \boldsymbol{H}_{\mathrm{T1}}^{\mathrm{diff2}t_{i+1}} & \cdots & \boldsymbol{H}_{\mathrm{T}N}^{\mathrm{diff2}t_{i+1}}\\ \vdots & \vdots & \\ \boldsymbol{H}_{\mathrm{T1}}^{\mathrm{diff}(m-1)t_{i+1}} & \cdots & \boldsymbol{H}_{\mathrm{T}N}^{\mathrm{diff}(m-1)t_{i+1}}\end{bmatrix}\\ &= \boldsymbol{L}_{\mathrm{T}}^{t_{i+1}} \oplus \mathcal{F}\left(\boldsymbol{K}_{m-1}^{t_{i+1}}\right)\end{aligned} \tag{8}$$

修正效果如图3所示，未修正的迭代时域算法经过modify函数处理后消除了与传统时域算法的偏差。

3.2 迭代模型的低复杂度近似

为减少计算复杂度，定义搜索函数sort_max$_{L-1}$，搜索各面元的反射信道中强度最大的$L-1$个反射信道，L为信道缓存长度，其取值由搜索出的反射信道强度与反射信道总强度的占比决定

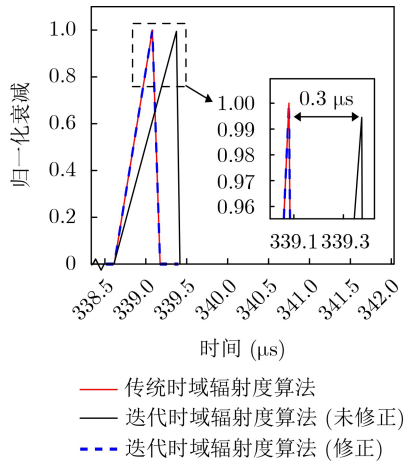

图 3 修正迭代时域辐射度算法的计算偏差

$$\begin{aligned}&\mathrm{sort\_max}_{L-1}\left(\mathcal{F}\left(\boldsymbol{K}_{m-1}^{t_i}\right)\right)\\&=\begin{bmatrix} j_{11}^{t_i} & \cdots & j_{N1}^{t_i}\\ \vdots & \ddots & \vdots\\ j_{1(L-1)}^{t_i} & \cdots & j_{N(L-1)}^{t_i}\end{bmatrix}\\&=\boldsymbol{J}^{t_i}\end{aligned}\tag{9}$$

其中，$\boldsymbol{J}^{t_i}$为t_i时刻每个面元强度最强的$L-1$个反射信道，之后利用modify函数对搜索出的信道进行修正

$$\begin{aligned}\mathrm{modify}\left(\boldsymbol{J}^{t_i}\right)&=\mathrm{modify}\left(\begin{bmatrix} j_{11}^{t_i} & \cdots & j_{N1}^{t_i}\\ \vdots & \ddots & \vdots\\ j_{1(L-1)}^{t_i} & \cdots & j_{N(L-1)}^{t_i}\end{bmatrix}\right)\\&=\begin{bmatrix} j_{11}^{t_{i+1}} & \cdots & j_{N1}^{t_{i+1}}\\ \vdots & \ddots & \vdots\\ j_{1(L-1)}^{t_{i+1}} & \cdots & j_{N(L-1)}^{t_{i+1}}\end{bmatrix}=\boldsymbol{J}_{\mathrm{mod}}^{t_{i+1}}\end{aligned}\tag{10}$$

$\boldsymbol{J}_{\mathrm{mod}}^{t_{i+1}}$为各面元经过修正后的反射信道，加上当前$t_{i+1}$时刻的直射信道后，将其定义为信道缓存$\boldsymbol{K}_{\mathrm{cache}}^{t_{i+1}}=\boldsymbol{L}_{\mathrm{T}}^{t_{i+1}}\oplus\boldsymbol{J}_{\mathrm{mod}}^{t_{i+1}}=\begin{bmatrix}\boldsymbol{L}_{\mathrm{T}}^{t_{i+1}}\\ \boldsymbol{J}_{\mathrm{mod}}^{t_{i+1}}\end{bmatrix}$。因此$t_{i+1}$时刻$\boldsymbol{K}_{\mathrm{cache}}^{t_{i+1}}$的计算过程表示为

$$\boldsymbol{K}_{\mathrm{cache}}^{t_{i+1}}=\boldsymbol{L}_{\mathrm{T}}^{t_{i+1}}\oplus\mathrm{modify}\left(\mathrm{sort\_max}_{L-1}\left(\mathcal{F}\left(\boldsymbol{K}_{\mathrm{cache}}^{t_i}\right)\right)\right)\tag{11}$$

最后将t_{i+1}时刻信道缓存$\boldsymbol{K}_{\mathrm{cache}}^{t_{i+1}}$中的信道向接收机反射，得到收发机间的信道$\boldsymbol{R}^{t_{i+1}}=\boldsymbol{K}_{\mathrm{cache}}^{t_{i+1}}\circledast\boldsymbol{L}_{\mathrm{R}}^{\mathrm{diag}}$，完成$t_{i+1}$时刻的计算。迭代时域辐射度算法的系统框图如图4所示。

4 计算仿真

算法的仿真实验采用500km×500km尺度的数字高程模型(Digital Elevation Model, DEM)构建战场环境。使用ArcMap地理数据处理软件，基于海拔差值对DEM数据执行Delaunay三角剖分算法，生成包含1 469个面元的三角网络模型[16]，如图5所示。

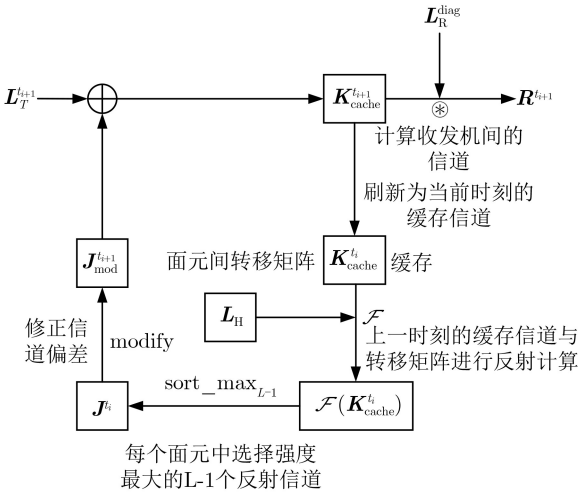

图 4 迭代时域辐射度算法系统框图

为平衡精度与复杂度，设置传统时域辐射度算法反射次数m为3。因计算机内存限制，频域辐射度算法采样点数P_{FFT}设置为256，对应时延分辨率为8 μs。迭代辐射度算法中，信道缓存中反射信道强度占比随L增加。随机选取100个坐标点模拟发射机部署位置，计算信道缓存中反射信道的强度占比，如图6所示，当缓存长度L为8时，占比超过98%，故后续仿真采用此设置。

图7(a)–图7(d)展示迭代时域辐射度算法计算下，场景中面元信道归一化强度从初始时刻开始前四个时刻的变化，反映信道多次反射过程。

图8对比了3种算法的计算结果，两种时域辐射度算法的结果(图8中红色虚线和蓝色实线)相近。相比于时域算法，频域辐射度算法的信道时延分辨率较低(图8中绿线)，无法区分时延差较小的信道。

多径信道的时延特性由平均时延$\overline{\tau}=\sum_{i=1}^{K}D_i\tau_i\Big/\sum_{i=1}^{K}D_i$和均方根时延扩展$\sigma_r=\sqrt{\sum_{i=1}^{K}D_i(\tau_i-\overline{\tau})^2\Big/\sum_{i=1}^{K}D_i}$表征，其中$D_i$为第$i$个信道的强度，$\tau_i$为相应的时延。随机设定100对收发机位置，迭代时域算法与传统时域算法在平均时延和均方根时延扩展上的平均偏差分别为0.04%和0.9%，显示出高一致性。

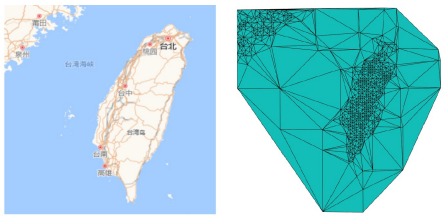

(a) 战场环境 (b) 三角网络模型

图 5 战场仿真场景三角网络模型

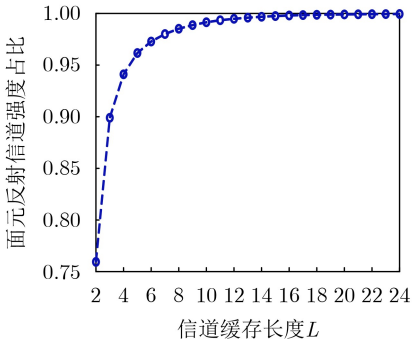

图 6 面元反射信道强度占比随着信道缓存长度的变化

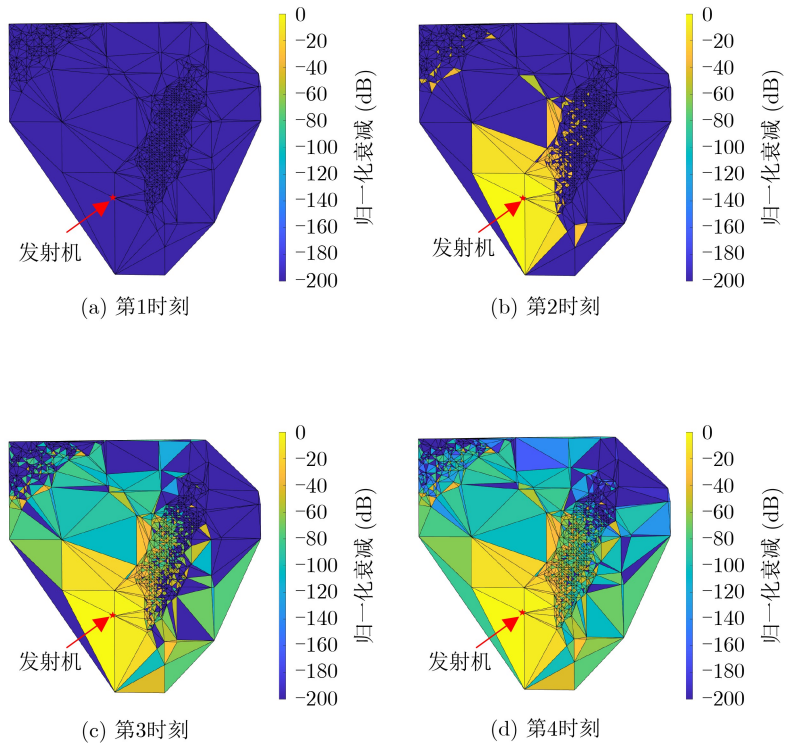

(a) 第1时刻　(b) 第2时刻

(c) 第3时刻　(d) 第4时刻

图 7 迭代辐射度算法面元中信道归一化衰减强度

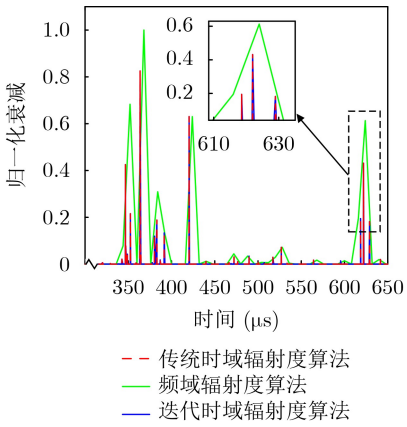

图 8 3种方法信道衰减和时延

3种算法的计算复杂度如表1所示，在面元数为N的场景中，传统时域辐射度算法的计算复杂度为$O(N^m)$，其复杂度随着反射次数m的增加呈指数提升。频域辐射度算法的计算复杂度为$O(N^2 \cdot P_{\mathrm{FFT}})$，其中$O(N^2)$为单个频点进行反射计算的复杂度，$P_{\mathrm{FFT}}$为频域辐射度算法中FFT点数。$P_{\mathrm{FFT}}$由场景中的传播时延上限和时延分辨率的比值决定，由于大尺度战场环境的空间尺度大导致传播时延上限高，要获得较高的时延分辨率，P_{FFT}需要被设置为较大的值，导致复杂度较高。在迭代时域辐射度算法中，$O(N^2 \cdot L)$为缓存长度为L的面元缓存与转移矩阵进行反射计算的复杂度，$O\left((NL) \cdot \log_2(L-1) \cdot N\right)$为选择面元中强度最大的$L-1$个反射信道的计算复杂度，因此总的计算复杂度为$O\left(N^2 \cdot L \cdot (\log_2(L-1)+1)\right)$。

表 1　算法的计算复杂度

算法名称	计算复杂度
传统时域辐射度算法	$O(N^m)$
频域辐射度算法	$O(N^2 \cdot P_{\mathrm{FFT}})$
迭代时域辐射度算法	$O\left(N^2 \cdot L \cdot (\log_2(L-1)+1)\right)$

在设置的仿真条件下，3种算法的计算复杂度如图9所示。

统计在MATLAB仿真中3种方法在面元数不同的战场环境中进行一个时刻计算的时间消耗，仿真平台处理器为第13代英特尔酷睿i7-13700H，内存为32 GB，计算时间如图10所示。

图10中迭代时域辐射度算法在计算时间上优于其他算法，且随着面元数量N增加，其速度优势更显著。在$P_{\mathrm{FFT}}=256$的情况下，频域辐射度算法的时延分辨率固定为8μs，不满足时延分辨率精度要求，而如果优化时延分辨率至纳秒级，P_{FFT}需扩大数百倍，导致计算时间大幅增加。

5　结论

为提升大尺度战场环境下电磁信道的计算速度，本文针对传统时域辐射度算法的计算复杂度大和频域辐射度算法的低时延分辨率问题，设计了一种迭代时域辐射度算法。仿真结果表明，本方法在

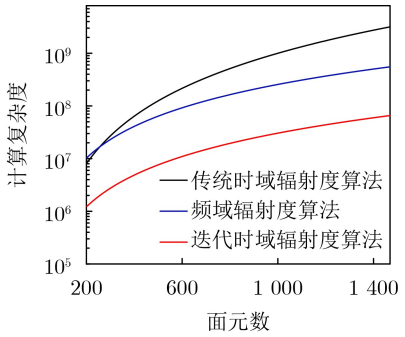

图 9 3种算法计算复杂度随面元数的变化

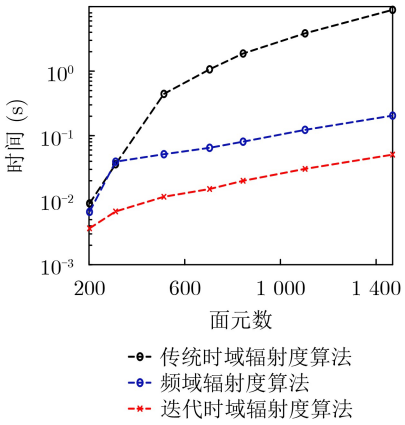

图 10 3种算法计算时间随面元数的变化

保证精度和高时延分辨率的同时显著提升了计算速度，满足了大尺度战场环境下信道的计算需求。

参 考 文 献

[1] TESTOLINA P, POLESE M, JOHARI P, *et al*. Boston twin: The Boston digital twin for ray-tracing in 6G networks[C]. Proceedings of the 15th ACM Multimedia Systems Conference, Bari, Italy, 2024: 441–447. doi: 10.1145/3625468.3652190.

[2] BAUMGÄRTNER L, BAUER M, and BLOESSL B. SUN: A simulated UAV network testbed with hardware-in-the-loop SDR support[C]. 2023 IEEE Wireless Communications and Networking Conference (WCNC), Glasgow, United Kingdom, 2023: 1–6. doi: 10.1109/WCNC55385.2023.10119014.

[3] VILLA D, TEHRANI-MOAYYED M, ROBINSON C P, *et al*. Colosseum as a digital twin: Bridging real-world experimentation and wireless network emulation[J]. *IEEE Transactions on Mobile Computing*, 2024, 23(10): 9150–9166. doi: 10.1109/TMC.2024.3359596.

[4] RUSCA R, RAVIGLIONE F, CASETTI C, *et al*. Mobile RF scenario design for massive-scale wireless channel emulators[C]. 2023 Joint European Conference on Networks and Communications & 6G Summit (EuCNC/6G Summit), Gothenburg, Sweden, 2023: 675–680. doi: 10.1109/EuCNC/6GSummit58263.2023.10188319.

[5] MOHANTI S, BOCANEGRA C, SANCHEZ S G, *et al*. SABRE: Swarm-based aerial beamforming radios: Experimentation and emulation[J]. *IEEE Transactions on Wireless Communications*, 2022, 21(9): 7460–7475. doi: 10.1109/TWC.2022.3158866.

[6] MUKHERJEE M, RAHMAN N M, DELUDE C, *et al*. A high performance computing architecture for real-time digital emulation of RF interactions[C]. 2023 IEEE Radar Conference (RadarConf23), San Antonio, USA, 2023: 1–6. doi: 10.1109/RadarConf2351548.2023.10149577.

[7] ERUNKULU O O, ZUNGERU A M, LEBEKWE C K, *et al*. Cellular communications coverage prediction techniques: A survey and comparison[J]. *IEEE Access*, 2020, 8: 113052–113077. doi: 10.1109/ACCESS.2020.3003247.

[8] KLOCH C, LIANG G, ANDERSEN J B, *et al*. Comparison of measured and predicted time dispersion and direction of arrival for multipath in a small cell environment[J]. *IEEE Transactions on Antennas and Propagation*, 2001, 49(9): 1254–1263. doi: 10.1109/8.947016.

[9] MONTIEL E, AGUADO A S, and SILLION F X. A radiance model for predicting radio wave propagation in irregular dense urban areas[J]. *IEEE Transactions on Antennas and Propagation*, 2003, 51(11): 3097–3108. doi: 10.1109/TAP.2003.818781.

[10] DU Kai, HUANG Huaguo, ZHU Yuyi, *et al*. Simulation of Ku-band profile radar waveform by extending radiosity applicable to porous individual objects (RAPID2) model[J]. *Remote Sensing*, 2020, 12(4): 684. doi: 10.3390/rs12040684.

[11] ALQUDAH Y A and KAVEHRAD M. MIMO characterization of indoor wireless optical link using a diffuse-transmission configuration[J]. *IEEE Transactions on Communications*, 2003, 51(9): 1554–1560. doi: 10.1109/TCOMM.2003.816945.

[12] FARAHNEH H, KHALIFEH A, and FERNANDO X. An outdoor multi path channel model for vehicular visible light communication systems[C]. 2016 Photonics North (PN), Quebec City, Canada, 2016: 675–680. doi: 10.1109/PN.2016.7537911.

[13] AYADI M, TORJEMEN N, and TABBANE S. Two-dimensional deterministic propagation models approach and comparison with calibrated empirical models[J]. *IEEE Transactions on Wireless Communications*, 2015, 14(10): 5714–5722. doi: 10.1109/TWC.2015.2442572.

[14] SCHULZE H. Frequency-domain simulation of the indoor wireless optical communication channel[J]. *IEEE Transactions on Communications*, 2016, 64(6): 2551–2562. doi: 10.1109/TCOMM.2016.2556684.

[15] SCHULZE H, MIETZNER J, and HOEHER P A. Dispersive optical wireless indoor channels–from frequency-

domain modeling to bit-error-rate prediction[J]. *IEEE Photonics Journal*, 2024, 16(1): 7300713. doi: 10.1109/JPHOT.2024.3357169.

[16] LIU Weirong, FEI Dan, GUAN Ke, *et al*. Channel measurements and modeling of wooded hilly terrain at sub-1 GHz band[J]. *IEEE Antennas and Wireless Propagation Letters*, 2024, 23(4): 1301–1305. doi: 10.1109/LAWP.2024.3353736.

刘　畅：男，博士生，研究方向为无线通信信号处理、无线信道建模等.

李维实：男，博士生，研究方向为射频电路系统、无线信道建模等.

徐　强：男，副研究员，研究方向为无线通信信号处理、太赫兹通信技术等.

时成哲：男，博士生，研究方向为通信抗干扰技术、相控阵天线技术等.

邵士海：男，教授，博士生导师，研究方向为无线通信信号处理、抗干扰与安全通信等.

责任编辑：余　蓉

Accelerated Channel Simulation Algorithm for Large-Scale Battlefield

LIU Chang　LI Weishi　XU Qiang　SHI Chengzhe　SHAO Shihai

(*National Key Laboratory of Wireless Communications*, *University of Electronic Science and Technology of China*, *Chengdu* 611731, *China*)

Abstract:

Objective　In large-scale battlefield environments, the testing and training of electromagnetic spectrum operation equipment rely on simulations within a vast digital electromagnetic environment. However, the computational complexity of large-scale electromagnetic channel simulations is high, hindering the improvement of computational speed. Traditional time-domain radiosity algorithms experience exponential growth in complexity with increasing reflection orders, while frequency-domain radiosity algorithms face limitations in time-delay resolution due to constraints in Fast Fourier Transform (FFT) points. This paper proposes an iterative time-domain radiosity algorithm that accelerates channel simulation, while maintaining high accuracy and time-delay resolution.

Methods　The proposed iterative time-domain radiosity algorithm uses a recursive modeling approach that reuses and corrects channel data from previous moments to reduce computational complexity. The algorithm begins by discretizing reflective surfaces in the environment into facets, which represent small, discrete elements capturing the reflective properties of the environment. The channel impulse response between the transmitter, facets, and receiver is modeled as a sum of direct and reflected components. The reflection process is described using shape factors that account for attenuation, delay, and visibility between facets, which are essential for accurately modeling interactions between the transmitter, facets, and receiver.To reduce computational complexity, the algorithm reuses channel data from the previous moment, leveraging small changes in the geographical location of the equipment between adjacent time steps. This reuse is possible due to the spatial coherence of the environment, ensuring that the previous channel data remains relevant with only minor adjustments. The channel data is then corrected by adjusting the delay and attenuation components based on changes in the direct shape factors between the transmitter and facets. This correction process ensures that the channel data remains accurate despite the reuse of prior calculations.The algorithm further employs a facet channel search method to approximate the channel by selecting the strongest reflection channels, thereby reducing the computational burden. This method involves identifying the top N strongest reflection channels within each facet, where N is determined by the desired balance between computational complexity and accuracy. By focusing on the strongest reflection channels, the algorithm significantly reduces the number of required calculations while maintaining high accuracy. The combination of data reuse, correction, and low-complexity approximation makes the proposed algorithm highly efficient for large-scale channel simulation.

Results and Discussions　Simulation results show that the proposed iterative time-domain radiosity algorithm improves computational speed by an order of magnitude, while maintaining accuracy, compared to the traditional time-domain radiosity algorithm (Fig. 10). This improvement is achieved by reusing and correcting channel data from previous moments, significantly reducing the number of recursive calculations required. The

enhanced computational speed is particularly crucial in large-scale battlefield environments, where traditional algorithms struggle with high computational complexity.In comparison to the frequency-domain radiosity algorithm, the proposed algorithm provides higher time-delay resolution, making it better suited for large-scale battlefield environments (Fig. 8). The time-delay resolution of the frequency-domain radiosity algorithm is constrained by the number of FFT points, which must be set to a large value to achieve high resolution in large-scale environments. In contrast, the iterative time-domain radiosity algorithm maintains high time-delay resolution without the need for large FFT points, making it more efficient for large-scale simulations.The computational complexity of the iterative time-domain radiosity algorithm is significantly lower than that of both the traditional time-domain radiosity algorithm and the frequency-domain radiosity algorithm (Table 1). The traditional time-domain radiosity algorithm's complexity grows exponentially with the number of reflections, while the iterative algorithm reduces complexity by reusing and correcting previous calculations. The frequency-domain radiosity algorithm also faces high complexity due to the large number of FFT points required for high time-delay resolution. The proposed algorithm's ability to reduce computational complexity while maintaining accuracy makes it a highly effective solution for large-scale channel simulations.Furthermore, the iterative time-domain radiosity algorithm demonstrates high consistency with the traditional time-domain algorithm in terms of average delay and root mean square delay spread, with average deviations of 0.04% and 0.9%, respectively. This indicates that the proposed algorithm preserves high accuracy while significantly improving computational efficiency. Its ability to accurately model the channel's time-delay characteristics is critical for applications in large-scale battlefield environments, where precise channel simulation is essential for the effective testing and training of electromagnetic spectrum operation equipment.

Conclusions The iterative time-domain radiosity algorithm proposed in this paper significantly enhances computational speed while maintaining accuracy and high time-delay resolution, addressing the computational challenges of channel simulation in large-scale battlefield environments. By reusing and correcting channel data from previous moments and employing a low-complexity approximation method, the algorithm reduces the computational burden without compromising accuracy. This makes it particularly well-suited for large-scale battlefield environments, where traditional algorithms struggle with high computational complexity and limited time-delay resolution. Future work could explore further optimizations and extend the algorithm to other electromagnetic environments, such as urban or indoor scenarios, where similar challenges in computational complexity and time-delay resolution may arise. Additionally, the algorithm could be adapted for real-time simulation systems, where rapid and accurate channel simulation is critical for decision-making and operational planning.

Key words: Channel simulation; Outdoor propagation; Radiosity